Energy dissipation of highly charged ions on Al oxide films

2010 J. Phys.: Condens. Matter 22 084008

(http://iopscience.iop.org/0953-8984/22/8/084008)

J. Phys.: Condens. Matter **22** (2010) 084008 (4pp) doi:10.1088/0953-8984/22/8/084008

Energy dissipation of highly charged ions on Al oxide films

R E Lake[1], J M Pomeroy[2] and C E Sosolik[1]

[1] Department of Physics and Astronomy, Clemson University, Clemson, SC 29634, USA
[2] National Institute of Standards and Technology (NIST), Gaithersburg, MD 20899, USA

E-mail: rlake@g.clemson.edu

Received 1 July 2009, in final form 25 August 2009
Published 4 February 2010
Online at stacks.iop.org/JPhysCM/22/084008

Abstract

Slow highly charged ions (HCIs) carry a large amount of potential energy that can be dissipated within femtoseconds upon interaction with a surface. HCI–insulator collisions result in high sputter yields and surface nanofeature creation due to strong coupling between the solid's electronic system and lattice. For HCIs interacting with Al oxide, combined experiments and theory indicate that defect mediated desorption can explain reasonably well preferential O atom removal and an observed threshold for sputtering due to potential energy. These studies have relied on measuring mass loss on the target substrate or probing craters left after desorption. Our approach is to extract highly charged ions onto the Al oxide barriers of metal–insulator–metal tunnel junctions and measure the increased conductance in a finished device after the irradiated interface is buried under the top metal layer. Such transport measurements constrain dynamic surface processes and provide large sets of statistics concerning the way individual HCI projectiles dissipate their potential energy. Results for Xe^{q+} for $q = 32, 40, 44$ extracted onto Al oxide films are discussed in terms of postirradiation electrical device characteristics. Future work will elucidate the relationship between potential energy dissipation and tunneling phenomena through HCI modified oxides.

1. Introduction

The interaction of slow highly charged ions (HCIs) with surfaces are intrinsically far-from-equilibrium situations, as the ions, stripped of a majority of their electrons, interact strongly in a high energy density collision. For example, on insulating surfaces, the large electronic potential energy of the HCI results in high sputter yields due to a many-body desorption process induced by electronic transitions involving hundreds of electrons per incident projectile. This potential sputtering by HCI impact leaves behind experimentally observable nanofeatures that form a record of this strong interaction [1, 2]. A formidable and ongoing theoretical problem is the development of a description for electronic sputtering of materials by slow HCIs. This description must account for the microscopic mechanisms that facilitate the transfer of an HCI's potential energy to the motion of sputtered particles and the subsequent creation of specific nanoscale features, such as craters or hillocks [3].

For a metal target surface, the relaxation of the electronic potential energy carried by a slow HCI from a high charge state q to a neutral state can be described via the classical over-the-barrier model [4]. At a critical distance from the surface, the ion captures electrons into high Rydberg states creating an electronic population inversion that is often called a hollow atom [5]. De-excitation of the hollow atom occurs by Auger electron emission, auto-ionization, and radiative decay processes [6]. The relaxation process continues as the ion impacts the surface, and any electrons still in highly excited states are screened by the surface electron gas. The filling of all remaining inner-shell vacancies occurs by direct electron transfer from the solid. During these relaxation steps, no significant dependence of the sputter yield on HCI charge state is observed experimentally as the electron gas in the metal can easily supply the electrons required to complete the neutralization process.

In contrast to the metal case, HCIs interacting with an insulator give a significant and measurable increase in sputter yield due to potential sputtering. These effects are enhanced for slow ions, as the potential energy is more important than kinetic energy in accounting for the observed yields [1]. In fact, for most insulators, the amount of material sputtered or the size of resulting nanofeatures increases monotonically with the increasing charge state (potential energy) of the incident

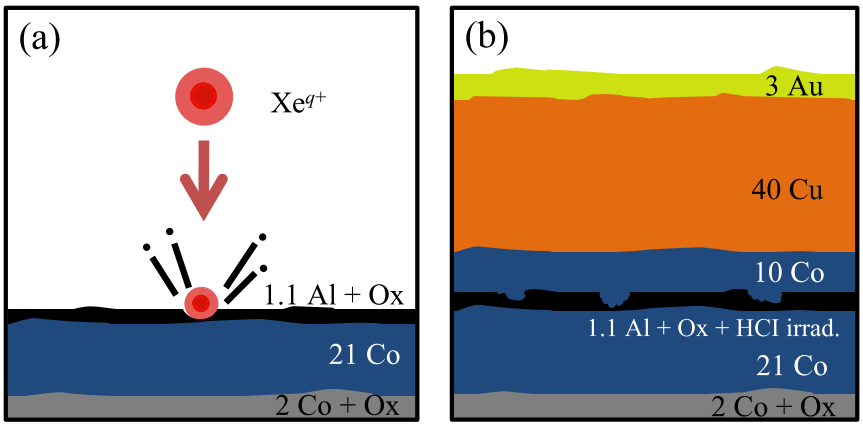

Figure 1. Experimental device schematic. (a) The bottom electrodes and AlO_x barrier were prepared and then irradiated with a beam of highly charged Xe^{q+} for $q = 32$, 40 and 44. (b) Immediately after ion irradiation the top metal electrode layers were deposited to complete the device. Layer thicknesses are given in nanometers and '+Ox' indicates that the O plasma oxidation procedure was performed after the metal layer was deposited.

(This figure is in colour only in the electronic version)

slow ions [2]. Many consider this behavior a technological opportunity to efficiently sputter the topmost layers of a surface without the radiation damage caused by the momentum cascade normally induced in swift ion impacts [1].

In considering HCI–insulator interactions, one must note that during the final part of a classical over-the-barrier relaxation process, the Coulombic potential energy of the HCI couples very strongly to the solid's electronic system. Previous descriptions of electron and photon stimulated desorption induced by electronic transitions (DIET) processes in alkali halides have utilized a defect mediated desorption model. This model has also been suggested for AlO_x, which is the target of interest in this work, as it is a similar material in terms of its wide band gap. Furthermore, its strong electron–phonon coupling implies that electronic excitations can be localized [7] to allow efficient energy transfer from the electronic to the phononic system of the solid [1].

Defect mediated desorption models have been invoked in order to explain reported preferential oxygen sputtering as well as the threshold behavior for the onset of potential sputtering for HCIs interacting with Al oxide [7, 8]. However, to the best of our knowledge, specific theoretical details for defect mediated desorption in Al oxide have yet to be calculated. These details include dependence of sputter yield on the stoichiometry of the Al oxide surface, the effect of AlO_x target thickness on defect formation (bulk and thin film limits), and the geometries of the nanofeatures produced after desorption has occurred. Technological uses of Al oxide motivate an understanding of electronic defect formation in this system [9]. To further elucidate electronic desorption processes for HCIs on AlO_x, we have exposed the thin AlO_x barriers of partially fabricated tunnel junctions to HCIs before depositing top metal electrodes [10, 11]. By measuring the increase in electrical transparency of each completed device due to the HCIs, information about the sizes and local electronic characteristics of nanofeatures can be deduced. These measurements complement previous sputter yield and scanning probe measurements [7, 8, 12] in studying the DIET process that gives rise to nanofeature formation in HCI–insulator interactions.

2. Experiment

Using the National Institute of Standards and Technology (NIST) electron beam ion trap (EBIT) facility we can extract HCI beams and prepare surfaces in the same vacuum system. Energetically resolved HCI beams with varying charge state q can be extracted onto multilayer metal oxide structures prepared entirely in ultrahigh vacuum [11, 13]. The EBIT employs a dense electron beam on the axis of a Penning trap-like electrode configuration to stepwise ionize the atoms in a gas to consecutively higher charge states. The trap electrode potentials can be set to a mode that leaks ions into the beamline. Prior to exposing the target to the beam, particles with the desired charge to mass ratio are selected. Under typical operating conditions, kinetic energy resolution has been measured to be $\Delta E/E < 1\%$. The target chamber is equipped with a Faraday cup for measuring HCI currents, a beam imaging system used for determining the beam size and approximate position, and an optical camera system for locating the precise position of the ion beam with a small aperture [11]. Current densities for the beams in this experiment were approximately 3–5 pA mm^{-2}. For the selected exposure time intervals, ion areal densities varied from less than ten ions per square micrometer to hundreds of ions per square micrometer.

Multiple tunnel junctions with the same device recipe were prepared with the layer structure: 2.0 Co + Ox/20.0 Co/1.0 Co/1.1 Al + Ox/10.0 Co/40.0 Cu/3.0 Au, where layers are listed from bottom to top and thicknesses are given in nanometers with '+Ox' indicating which layers were plasma oxidized (figure 1). Samples consisted of four tunnel junction devices arranged in a crossed wire geometry where top and bottom metal electrode wires were perpendicular to each other and each contacted opposite sides of the insulating AlO_x

barrier [11]. The points of intersection formed four metal–insulator–metal tunnel junctions.

The fabrication and irradiation processes were performed as follows. Pre-oxidized SiO_2 chips were introduced into the vacuum system load lock where O plasma cleaning cycles were performed. After cleaning, the chips were transferred into the deposition chamber that was equipped with a five pocket electron beam evaporator. Depositions were monitored with a quartz crystal oscillator and controlled by a pneumatic shutter between the evaporant and substrate. The typical pressure in the deposition chamber during film growth was 10^{-6} Pa.

A 2.0 nm base layer of Co was deposited onto each chip and then oxidized by exposure to O plasma for 20 s. Bottom Co electrodes were deposited on the oxidized Co base layer through a shadow mask forming the bottom wire that was (90± 8) μm wide. Afterward, the Al layer was deposited without a mask, followed by plasma oxidation to fully oxidize the Al and form the amorphous Al oxide tunnel barrier. Batches of eight chips were prepared up to the Al oxide layer and stored overnight at room temperature in a UHV (10^{-7} Pa) chamber prior to HCI beam exposure.

A beam of highly charged ions with $q = 32$, 40 or 44 was extracted onto each AlO_x thin film barrier for times between 30 and 2000 s near normal incidence. HCI kinetic energies were $(8.1 \times q)$ keV giving a variation in kinetic energy between 259 and 356 keV for the beams described here. Simulated stopping power variation for this kinetic energy difference on an Al oxide surface varies only between 4.57 and 4.61 keV nm^{-1} [14] while the electronic potential energies of these three charge states are 19.3, 38.7 and 51.3 keV. Each device on a chip was independently exposed to HCIs, and one device per chip was always left unexposed as a control. Immediately after irradiation, the top metal electrodes were deposited onto the AlO_x surface through another shadow mask to form (90±8) μm wide top wires perpendicular to the bottom electrodes: 10.0 nm Co, 40.0 nm Cu, 3.0 nm Au (figure 1). Once a chip was complete (figure 1(b)), it was removed from vacuum and measured using a four-point resistance technique. After correcting for a geometric artifact [15], the inverse of the four-point resistance was taken to be the electrical conductance G of a device. Additionally, the differential conductance $(\mathrm{d}I/\mathrm{d}V)$ as a function of bias voltage was measured for each device. Figure 2 shows a differential conductance curve for a device irradiated with ions with $q = 32$, as well an unirradiated control device.

3. Results and discussion

For tunnel junctions described here, the electrical transparency of the devices always increases after HCI irradiation of the insulating barrier. The observed conductance increase in the devices indicates barrier thinning because the electron tunneling probability is exponentially sensitive to the thickness of the barrier. When HCIs impinge on the surface of the insulator (figure 1 (a)), they sputter atoms on the AlO_x surface through a potential energy induced desorption process causing ablation and rearrangement of surface atoms [7, 8]. As our measurements of irradiated tunnel junctions cannot be explained without some fundamental reduction in the barrier thickness, we refer to a single modification on the insulator as a crater. The irradiated barrier is modified by the formation of craters that dramatically increase its electrical transparency due to a local reduction in the barrier thickness, a reduction of the insulating barrier energy height, or some convolution of the two. We note there is an active discussion about how specific desorption processes lead to the hillocks or craters observed for different materials [2]. A previous experimental investigation of crystalline $Al_2O_3(0\ 0\ 0\ 1)$ reports hillock formation by atomic force microscopy measurements in experiments with Ar^{q+} and charge states up to $q = 7$ [12].

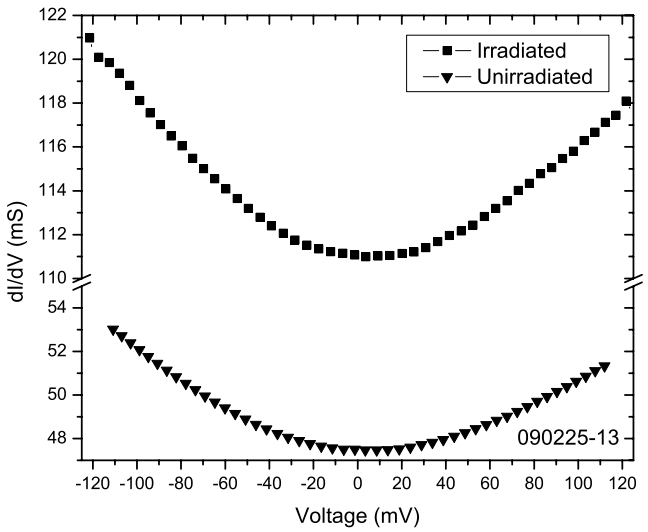

Figure 2. Corrected [15] differential conductance curves for an unirradiated device and a device irradiated with Xe^{32+} ions. Both devices maintain the same non-linear $\mathrm{d}I/\mathrm{d}V$ behavior characteristic of tunneling transport with the same relative curvatures. HCI irradiation of the barrier increases the conductance of the device by more than a factor of two.

In our model, each crater contributes a finite amount to the overall conductance of a device and we fit the data to the linear function $G = \sigma_c N + G_0$. The slope of the fit σ_c is the increase in conductance per HCI impact on the barrier and G_0 is the original undosed conductance of a device (figure 3). In this way, we probe potential energy dissipation by measuring an ensemble average of increased tunnel junction conductance for individual HCIs of a given q on AlO_x thin films.

Figure 2 displays the differential conductance as a function of bias voltage characteristics of a device irradiated by Xe^{32+} and an unirradiated tunnel junction. The data for the irradiated device have a similar parabolic dependence, and the differential conductance curves maintain the same relative curvature before and after irradiation. Therefore, we conclude that most ions do not breach the barrier to create Ohmic contacts between the top and bottom electrodes [9]. The similarity of the $\mathrm{d}I/\mathrm{d}V$ curvatures for the devices in figure 2 also indicates that the device barrier height in energy does not change significantly and implies that we do not observe a change in stoichiometry for the irradiated barrier.

Figure 3 shows $G(N)$ data for two different charge states $q = 40$ and 44. After resistance measurement of the tunnel

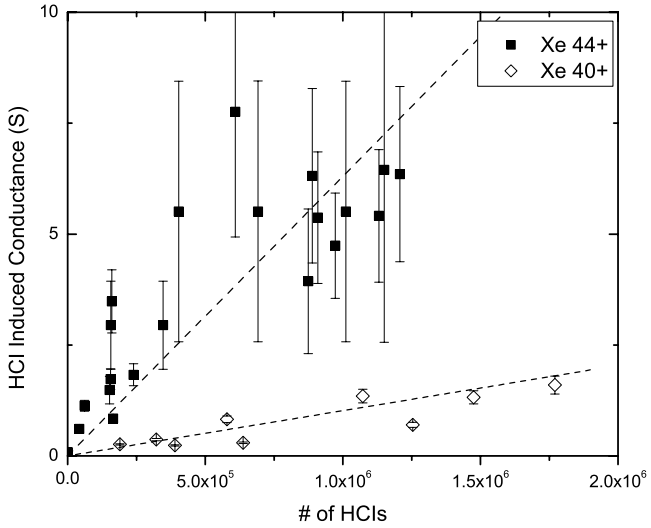

Figure 3. $G(N)$ for $q = 40$ and 44. The slopes of these linear fits σ_c are the increase in device conductance per ion impact on the Al oxide barrier.

junctions, these data were corrected to account for a geometric 'negative resistance' artifact. Because this error is non-linear and has a greater relative effect on devices with low resistance (high conductance), error bars for the $q = 44$ irradiated devices are greater than the $q = 40$ set [15]. From $q = 40$ to 44, σ_c increases by a factor of approximately 6. This is to be expected as nanofeature sizes on insulators created by HCIs generally increase with potential energy [2]. The charge states shown in figure 3 are consistent with this behavior indicating that in the region of a HCI impact, the barrier thickness is decreased by the radius of a crater. The sensitivity of the barrier to HCI impact and therefore the slope of the $G(N)$ plot also depends on the initial resistance–area product of the device due to the fundamental exponential dependence of electron tunneling probability on the thickness of the insulating barrier [10].

While measuring the conductance of a tunnel junction with an irradiated barrier is an indirect method of probing the HCI desorption process, it complements earlier mass loss and direct scanning probe measurements [7, 12]. Measuring transport through a tunnel junction provides large sets of statistics for DIET events initiated by a certain HCI charge state. Also, time dependent surface processes that could affect direct measurements of craters can be constrained by immediately depositing a metal film onto the Al oxide surface. Devices in a batch all have the same environmental history and the buried metal–insulator interface is stable. Descriptions of how microscopic roughness fluctuations on a buried interface can affect the macroscopic observables of a device may offer new insight into understanding the effect of the HCIs on the barrier [16]. Changing the charge state of HCIs tunes the energy density of electronic excitations and allows a systematic indirect method of probing the DIET processes that cause potential sputtering.

4. Conclusion

In conclusion, we have discussed our approach that uses tunnel junctions to study the DIET process that occurs when HCIs neutralize at the surface of Al oxide films. This method is consistent with previous studies of HCI induced mass loss and nanofeature creation on insulators as we found that σ_c increases with the potential energy of the incident HCI for Xe^{q+} where $q = 34$, 40 and 44. σ_c is interpreted as the mean contribution from each ion to the total increased conductance of a tunnel junction for a given projectile potential energy. Future work will investigate σ_c over a greater range of q and model the conductance of irradiated tunnel junctions in the framework of tunneling transport theory.

Acknowledgments

The authors gratefully acknowledge support from National Science Foundation (NSF-CHE-0548111), NASA (Contract No. 2096693), and COMSET at Clemson University.

References

[1] Aumayr F and Winter H P 2004 *Phil. Trans. R. Soc.* A **362** 77
[2] Aumayr F, El-Said A S and Meissl W 2008 *Nucl. Instrum. Methods Phys. Res.* B **266** 2729
[3] Schenkel T, Hamza A V, Barnes A V and Schneider D H 1999 *Prog. Surf. Sci.* **61** 23
[4] Burgdörfer J, Lerner P and Meyer F W 1991 *Phys. Rev.* A **44** 5674
[5] Briand J P, Thuriez S, Giardino G, Borsoni G, Froment M, Eddrief M and Sébenne C 1996 *Phys. Rev. Lett.* **77** 1452
[6] Beyer H F and Shevelko V P 2003 *Introduction to the Physics of Highly Charged Ions* (Boca Raton, FL: CRC Press)
[7] Hayderer G, Cernusca S, Hoffmann V, Niemann D, Stolterfoht N, Schmid M, Varga P, Winter H P and Aumayr F 2001 *Nucl. Instrum. Methods Phys. Res.* B **182** 143
[8] Hayderer G, Cernusca S, Schmid M, Varga P, Winter H, Aumayr F, Niemann D, Hoffmann V, Stolterfoht N, Lemell C, Wirtz L and Burgdrfer J 2001 *Phys. Rev. Lett.* **86** 3530
[9] Pomeroy J M, Grube H, Perrella A C and Gillaspy J D 2007 *Appl. Phys. Lett.* **91** 073506
[10] Pomeroy J M and Grube H 2009 *Nucl. Instrum. Methods Phys. Res.* B **267** 642
[11] Pomeroy J M, Grube H and Perrella A C 2007 *Radiat. Eff. Defects Solids* **162** 473
[12] Gebeshuber I C, Cernusca S, Aumayr F and Winter H 2003 *Nucl. Instrum. Methods Phys. Res.* B **205** 751
[13] Ratliff L P, Bell E W, Parks D C, Pikin A I and Gillaspy J D 1997 *Rev. Sci. Instrum.* **68** 1998
[14] Ziegler J F and Biersack J P 2006 *SRIM* http://www.srim.org
[15] Pomeroy J M and Grube H 2009 *J. Appl. Phys.* **105** 094503
[16] Da Costa V, Henry Y, Bardou F, Romeo M and Ounadjela K 2000 *Eur. Phys. J.* B **13** 297